Available online at www.sciencedirect.com
ScienceDirect
Procedia CIRP 45 (2016) 43 – 46
www.elsevier.com/locate/procedia

3rd CIRP Conference on Surface Integrity (CIRP CSI)

Material modifications caused by thermal and mechanical load during grinding

S. Jermolajev[a]*, J. Epp[b], C. Heinzel[a], E. Brinksmeier[a]

[a]*Foundation Institute of Materials Science (IWT), Division Manufacturing Technologies and University of Bremen, MAPEX Center for Materials and Processes, Badgasteiner Str. 3, 28359 Bremen, Germany*
[b]*Foundation Institute of Materials Science (IWT), Division Materials Science and University of Bremen, Badgasteiner Str. 3, 28359 Bremen, Germany*

* Corresponding author Tel.: +49 (0)421 218 51183; fax: +49 (0)421 218 51102. E-mail address: jermolajev@iwt-bremen.de.

Abstract

This paper discusses results acquired during surface grinding experiments performed on hardened steel workpieces. The experimental results show different zones of thermally induced material modifications during grinding depending on the contact time Δt and the maximum contact zone temperature T_{max}. In particular it was observed that rehardened zones occurred within two separated ranges of temperatures and contact times. Further analyses revealed that these separated time and temperature ranges correspond to significantly different mechanical loads as well as to varying retained austenite rates. The experimental results shall help to identify possible mechanisms responsible for the observed material modifications during grinding.

Peer-review under responsibility of the scientific committee of the 3rd CIRP Conference on Surface Integrity (CIRP CSI)
Keywords: Grinding, Residual stress, Surface integrity, Thermal effects

1. Objectives and general research approach

The grinding process can be considered as an external short-time local thermo-mechanical load on the workpiece surface [1]. This load results from the engagement between the ground workpiece surface and the single abrasive grains at the surface of the grinding wheel. Due to the high velocity and the multiplicity of the abrasive grains, the external workpiece surface load can be characterized by local „flash" temperatures and grinding forces [2]. This would imply local peak temperatures and stresses near the workpiece surface as well. However, experimental investigations, for example according to [3], indicated rather continuously increasing temperatures and stresses beneath the workpiece surface. The determination of internal thermal loads has been subject to numerous investigations, since it primarily affects the resulting surface layer properties of the ground workpiece [1, 4, 5].

This paper refers to long-term research efforts aiming at the identification and the prediction of the internal thermal and mechanical material load during the grinding process. It is intended to correlate the internal material load to the modifications of workpiece surface layer properties after grinding (referred to as material modifications after [1]) by a physical based approach.

Since the thermal load during grinding primarily limits the workpiece quality (due to the onset of grinding burn), the focus of the experiments was laid on identifying the thermal load first. In previous investigations reported in [6], an approach based on the known TTA- and TTT-diagrams from the conventional heat treatment provided promising results. This approach is based on mapping the resulting material modifications over the maximum contact zone temperature T_{max} and the contact time Δt. This leads to the so called T_{max}-Δt-diagram (cf. figure 1). The contact time Δt can be calculated according to the following expression:

$$\Delta t = \frac{l_g}{v_{ft}}, \tag{1}$$

where l_g denotes the geometric contact length and v_{ft} denotes the tangential feed speed. The primary purpose of the T_{max}-Δt-diagram is to achieve targeted material modifications after grinding by means of in-process temperature monitoring.

Peer-review under responsibility of the scientific committee of the 3rd CIRP Conference on Surface Integrity (CIRP CSI)
doi:10.1016/j.procir.2016.02.159

When established, the application of the T_{max}-Δt-diagram saves additional experiments which would be necessary to find a suitable process layout leading to the desired material modifications.

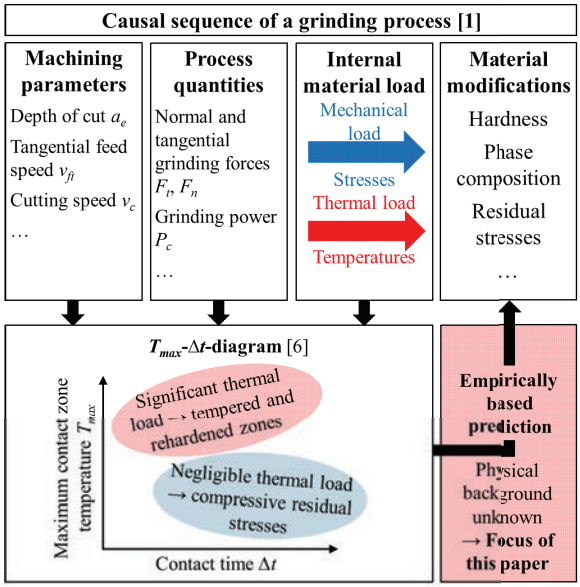

Fig. 1. T_{max}-Δt-diagram - a simplified empirical approach to predict material modifications after grinding.

In the following sections, a new T_{max}-Δt-diagram for the workpiece material 16MnCr5 (AISI 5115) identified during surface grinding experiments is discussed. This discussion goes along with considerations referring to the possible phase transformations due to the internal thermal material load as well as to the mechanical load during grinding. These considerations shall help to understand the physical background of the material modifications mapped in the presented T_{max}-Δt-diagram.

2. Experimental results

In order to identify the T_{max}-Δt-diagram for 16MnCr5, a series of surface grinding experiments was performed (cf. figure 2). In order to investigate an interval of T_{max}-values and Δt-values which should be as large as possible, the depth of cut a_e was increased up to its maximum value during a single experiment (v_{ft} was being held constant). A further extension was achieved by performing multiple experiments with different tangential feed speeds v_{ft} and with different coolant flow rates delivered by the coolant nozzle. In order to reduce the effect of grinding wheel clogging and to enhance the reproducibility of the grinding experiments, an additional high pressure cleaning nozzle was used.

During each grinding experiment, the maximum contact zone temperature T_{max} was measured by a temperature measurement system as introduced in [7]. This system is based on the evaluation of the infrared radiation emitted by the ground workpiece surface within the contact zone. A part of the infrared spectrum (wavelength between 2 µm and 4 µm) is transferred to the IR-photodiode which transforms it into an electrical signal. The electrical signal is pre-processed and the values of T_{max} are sent wireless to the external computer. The measured T_{max}-values allow a comparison of the thermal load during grinding resulting from different process layouts. A direct correlation between the measured T_{max}-values and the actual workpiece temperatures during grinding is difficult [7], since the exact emissivity of the ground workpiece surface within the contact zone as well as the effect of grinding chips on the T_{max}-values are currently unknown. Therefore, in this paper, arbitrary units for T_{max} are used.

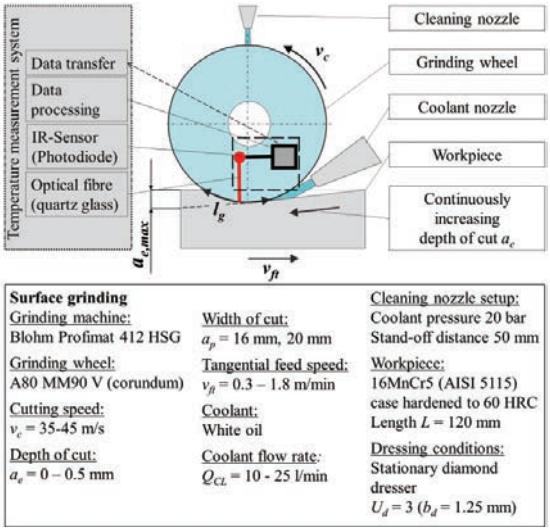

Fig. 2. Process layout of the performed surface grinding experiments.

The ground workpieces were analyzed by means of Barkhausen noise measurement, X-ray diffraction measurement as well as hardness measurement and metallographic inspection. In correspondence with previous work focused on the material modifications after grinding (for example [8]), areas of similar material modifications were defined (cf. table 1). The changes $\Delta\sigma_{RES}$ of resulting tangential surface residual stresses (referred to as residual stresses in the following sections) were calculated by considering the depth profile of residual stresses before grinding. Other criteria were the full width at half maximum FWHM resulting from the X-ray measurement, the Barkhausen noise level (BH), the hardness and optical micrographs.

By coupling the information on resulting material modifications with the measured T_{max}-values and the calculated Δt-values, the T_{max}-Δt-diagram for 16MnCr5 was established (see figure 3). The areas in this diagram are highlighted by a color code according to table 1.

It was found that the thermal impact of the grinding process may be kept minimal at contact times between 0.5 and approximately 1.20 s. By short contact times (below 0.50 s) and longer contact times as well (over 1.20 s), a stronger thermal impact was detected leading to tensile residual stresses. This corresponds to practical experience in grinding of various case hardened steels and reveals that choosing short contact times (which means lower depths of cut or higher tangential feed speeds) does not always ensure a „burn-free" grinding process. At higher contact zone temperatures, tempered zones were detected for almost the entire range of investigated contact times.

By a further increase of the contact zone temperatures, rehardened zones were detected as well. The rehardened zones occured at shorter contact times up to 0.70 s and at longer contact times over 1.00 s as well. The contact zone temperatures leading to the onset of rehardened zones are slightly decreasing at increasing contact times.

Table 1. Areas of similar material modifications after grinding 16MnCr5.

	$\Delta\sigma_{RES}$ [MPa]	FWHM [°]	BH [mV]	Hardness	Metallogr. inspection
Initial state (16MnCr5, case hardened)	-250 to -150	2.4	-	60 HRC	-
Area of compressive res. stresses	-200 to 0	over 6	no changes	no changes	no changes
Area of growing thermal impact	-200 to 0	decrease by 0.03 to 0.1	slight increase	no changes	no changes
Area of tensile residual stress	over 0	decrease by more than 0.1	increase to maximum	no changes	no changes
Area of tempered zones	20 to 400	decrease by more than 0.2	decrease	decrease (below 45 HRC)	dark etching areas
Area of rehardened zones	below -200	increase over 5.0	significant decrease	increase over 64 HRC	white etching areas

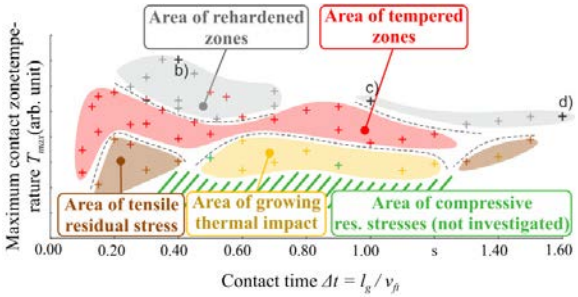

Fig. 3. T_{max}-Δt-diagram for 16MnCr5 (b, c, d – samples investigated in chapter 3).

Since the onset of rehardened zones has to be preceeded by the austenitisation of the workpiece surface layer, a significant increase of contact zone temperatures would rather be expected at shorter contact times due to the shift of the Ac_1-temperature to higher values with increasing heating rate, as known from the TTA-diagrams (Time-Temperature-Austenitisation) [9]. However, a major difference compared to conventional heat treatments for which the TTA-diagrams were developed is the presence of the external mechanical load. The mechanical impact may significantly affect the transformation temperatures. In particular, the hydrostatic pressure can reduce significantly the thermodynamic equilibrium temperature (Ac_1) down to 620°C for 5000 MPa of pressure due to a shift of the Gibbs free energy as shown in [10].

3. Microstructural changes in rehardened zones

In order to evaluate the impact of the grinding process on the microstructural changes in rehardened zones, metallographic inspections were performed by optical microscopy after polishing and etching using 3%-HNO_3-ethanol solution, as well as by Vickers microhardness profiles.

Figure 4 shows the optical micrographs of 3 different rehardened states located on the left (b), the center (c) and the right (d) of the rehardened region in the T_{max}-Δt-diagram (figure 3) compared to the initial state (a). Before grinding a typical microstructure consisting of tempered martensite and high amount of retained austenite can be observed. On the other hand, the microstructures of the three rehardened zones have a very fine morphology which is hard to resolve. The micrographs b and d seem to have a higher amount and larger regions of retained austenite (appearing in white) than c.

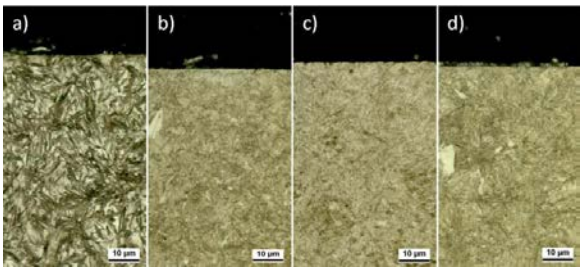

Fig. 4. Optical micrographs of three different rehardened zones compared to the initial state: a) before grinding; b) Δt = 0.4 s, c) Δt = 1.0 s, d) Δt = 1.6 s.

The microhardness profiles of the same four samples show that the surface hardness level and the affected depth (limit set at 550 HV1) is different for the different states with 730 HV1 and a case hardening depth (CHD) of 1.2 mm before grinding, 865 HV1 and a depth of 0.37 mm for figure 4b, 770 HV1 with a depth of 0.13 mm for figure 4c and finally, 856 HV1 and an affected depth of 0.55 mm for figure 4d.

Additionally, quantitative phase analyses were done by X-ray diffraction in order to determine precisely the amount of retained austenite. The measurements were made using a vanadium-filtered Cr-kα radiation from 60° to 164° 2θ and a beam size of Ø 2 mm. Based on the evaluation of the diffraction pattern, the martensite tetragonality due to the splitting of the diffraction peaks could be identified as well.

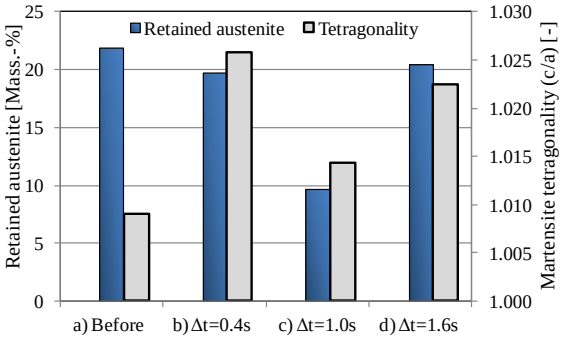

Fig. 5. Results of X-ray diffraction analyses performed at the samples presented in figure 4.

The results in figure 5 show that before grinding, a high amount of retained austenite is present together with a low tetragonality of the martensite as a consequence of the tempering process after case hardening. For the three rehardened zones, the martensite tetragonality which is directly related to the carbon content in solution, is

significantly increased due to the fact that the martensite present has not been tempered after formation. However, variations can be observed between the three rehardened samples. The samples b and d that exhibit the highest tetragonality (and therefore the highest carbon content in solution) have a high surface hardness and a high amount of retained austenite. On the other hand, the sample c which shows only a slight increase of tetragonality (low amount of carbon in solution) have a much lower hardness and a smaller rehardened depth together with a low amount of retained austenite.

4. Investigation of the mechanical impact during grinding

In order to investigate the effect of the external mechanical load during grinding on the onset of rehardened zones and the microstructural changes described in chapter 3, a simplified approach is proposed. This approach works with an approximation of the local surface related mechanical stress by using the average contact zone pressure p_n between the engaging abrasive grains and the ground workpiece surface.

$$p_n = \frac{F_n}{k_c \cdot l_g \cdot a_p}, \quad (2)$$

The coefficient k_c expresses the fraction of the total abrasive grain area which is in contact with the ground workpiece surface. Since the exact value of k_c is unknown, the absolute values of p_n could not be evaluated. Because of this, a reference range of p_n-values (p_{n0}) was identified. The other p_n-ranges were found by relating the characteristic p_n-values to the reference value p_{n0}.

By applying the presented approach for the experiments presented in figure 2, areas of p_n-values could be identified as shown in figure 6.

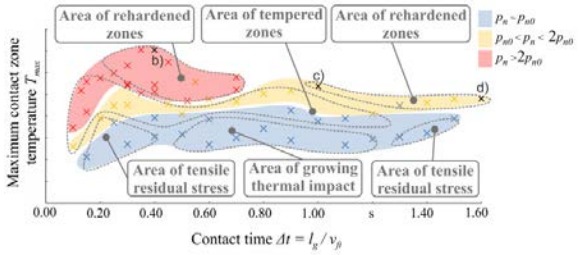

Fig. 6 Areas of p_n-values in the T_{max}-Δt-diagram for 16MnCr5 (b, c, d – samples investigated in chapter 3).

In the T_{max}-Δt-diagram in figure 6, the areas of p_n-values are mapped together with the resulting material modifications after grinding. It can be seen that the areas of rehardened zones at short contact times (below 0.70 s) and at long contact times (1.00 s and more) can be characterized by different p_n-ranges. With reference to the microstructure examination described in chapter 3, the sample c differs significantly from the samples b and d. This would suggest that the mechanical impact would not have a significant effect on the occurance and the depth of the rehardened zones observed at the samples b, c and d. However, it has to be considered that the k_c-values vary throughout the whole interval of investigated contact times, and thus, the actual local pressure between the single abrasive grains and the ground workpiece surface may differ from the tendencies shown in figure 6 based on the assumption of a constant k_c.

5. Summary and outlook

As the presented investigations show, the resulting material modifications after grinding 16MnCr5 can be characterized by temperature and contact time areas in the T_{max}-Δt-diagram. It was shown also that the structural state and the depth of the rehardened zones may vary at different T_{max}- and Δt-values within the corresponding areas in the T_{max}-Δt-diagram. For a more precise identification of the resulting material modifications after grinding, absolute workpiece contact zone temperatures as well as actual local mechanical stresses will have to be identified.

In the future works, an extended T_{max}-Δt-p_n-diagram will be sought which works with absolute workpiece temperatures during grinding and with local mechanical stresses within the contact zone between the abrasive grains and the workpiece material.

Acknowledgements

The authors express their sincere thanks to the Deutsche Forschungsgemeinschaft (DFG) for funding the subprojects F06 and C01 within the transregional collaborative research center SFB/TRR 136.

References

[1] Brinksmeier, E., Klocke, F., Lucca, D.A., Sölter, J., Meyer, D., Process Signatures – a new approach to solve the inverse surface integrity problem in machining processes, Procedia CIRP, Volume 13/2014. pp. 429-434.
[2] Malkin, S., Grinding Technology – Theory and Applications of Machining with Abrasives, Second Edition, Industrial Press, New York, 2008.
[3] Rowe, W. B., Morgan, M. N., Black, S. C: E., Mills, B., A Simplified Approach to Control of Thermal Damage in Grinding, CIRP Annals – Manufacturing Technology, Volume 45/1, 1996. pp. 299-302.
[4] Sakakura, M., Ohnishi, T., Shinoda, T., Ohashi, K., Tsukamoto, S., Inasaki, I., Temperature distribution in a workpiece during cylindrical plunge grinding, Production Engineering, Volume 6, Issue 2, 2012. pp. 149-155.
[5] Schulze, V., Uhlmann, E., Mahnken, R., Menzel, A., Biermann, D., Zabel, A., Bollig, P., Ivanov, I. M., Cheng, C., Holtermann, R., bartel, T., Evaluation of different approaches for modeling phase transformations in machining simulation, Production Engineering, Volume 9, Issue 4, 2015. pp. 437-439.
[6] Jermolajev, S., Brinksmeier, E., A new approach for the prediction of surface and subsurface properties after grinding, Advanced Materials Research, Volume 1018, 2014. pp. 189-196.
[7] Brinksmeier, E., Eckebrecht, J., Wilkens, A., Wheel Based Temperature Measurement in Grinding, Advanced Materials Research, Vol. 325/2011. pp. 3-11.
[8] Aurich, J. C., Linke, B., Hauschild, M., Carrella, M., Kirsch, B., Sustainability of abrasive processes, CIRP Annals – Manufacturing Technology, Volume 62/2013. pp. 653-672.
[9] Roos, E., Maile, K., Werkstoffkunde für Ingenieure, 4. edition, Springer Verlag, Berlin Heidelberg, 2011.
[10] Hilliard, J.E., The effect of high pressures on transformation rates. Trans. AIME, Volume 227, 1963. pp. 429-438.